

LA-8790

4.3

CIC-14 REPORT COLLECTION

REPRODUCTION
COPY

Los Alamos National Laboratory is operated by the University of California for the United States Department of Energy under contract W-7405-ENG-36.

*Experimental Model Study of
Initiation and Detonation in
Small PENT-Loaded Assemblies*

LOS ALAMOS NATIONAL LABORATORY
3 9338 00307 2062

Los Alamos Los Alamos National Laboratory
Los Alamos, New Mexico 87545

This work was supported by the US Department of the Navy, Strategic Systems Project Office.

Edited by Sharon Crane
Photocomposition by Kathy E. Valdez

DISCLAIMER

This report was prepared as an account of work sponsored by an agency of the United States Government. Neither the United States Government nor any agency thereof, nor any of their employees, makes any warranty, express or implied, or assumes any legal liability or responsibility for the accuracy, completeness, or usefulness of any information, apparatus, product, or process disclosed, or represents that its use would not infringe privately owned rights. References herein to any specific commercial product, process, or service by trade name, trademark, manufacturer, or otherwise, does not necessarily constitute or imply its endorsement, recommendation, or favoring by the United States Government or any agency thereof. The views and opinions of authors expressed herein do not necessarily state or reflect those of the United States Government or any agency thereof.

LA-8790

UC-45

Issued: July 1981

A Numerical Model Study of Burning and Detonation in Small PETN-Loaded Assemblies

Charles A. Forest



LOS ALAMOS NATL LAB. LIB.
3 9338 00307 2062

A NUMERICAL MODEL STUDY OF BURNING AND DETONATION IN SMALL PETN-LOADED ASSEMBLIES

by

Charles A. Forest

ABSTRACT

A simple model has been used in the 2DL code to calculate the burning and detonation in Robert Dinegar's all-PETN hot-wire assemblies. The model includes (1) a constant velocity ignition front, (2) conductive $\dot{X} = BP^n$ burn of particles behind the ignition front, (3) inertial confinement, and (4) shock initiation of detonation in the assembly transition tube PETN charge. The surface-to-volume ratio of the burning particles and the ignition front velocity were varied in a parameter study of the model.

I. INTRODUCTION

An explosive that is initially burning may sometimes detonate; the behavior change is called the deflagration-to-detonation transition (DDT). The term is non-specific and is used in a variety of circumstances occurring in explosive gases, liquids, solids, and mixtures of these phases. The DDT is considered contributory in some explosive accidents. However, DDT may also be used in design applications of explosive devices.

This report describes a model study for the deflagration-to-detonation transition in pressed secondary explosive. In particular, the study is restricted to one of the hot-wire-ignited, PETN-loaded experimental devices studied by Robert Dinegar.¹

II. THE EXPERIMENTAL ASSEMBLY

The PETN-loaded, hot-wire-ignited, SE-1 assembly is shown in Fig. 1. This device uses an SE-1 detonator mechanical assembly, which includes the plastic head with mounted bridgewire and the brass tube, interior to a steel confining jacket. The SE-1 is loaded partially with pressed PETN, the donor charge. Atop the donor charge

is a steel tube loaded with PETN pressed to a lower density, the transition charge. The steel transition tube fits inside the brass SE-1 tube and confines the donor charge. The reduced inside diameter of the transition

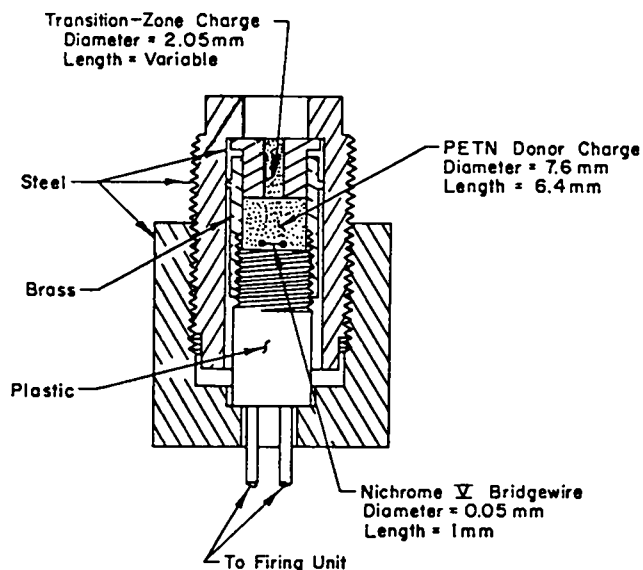


Fig. 1.

Hot-wire-ignited DDT assembly (Dinegar).

tube is necessary to the functioning of the device. The assembly is fired by heating electrically, but not exploding, the bridgewire.

Dinegar varied the pressing densities. The donor charge was pressed to 1.40 and 1.60 g/cm³. The transition charge was pressed to densities of 0.8, 1.00, 1.20, 1.40, and 1.60 g/cm³. Successful detonations were produced with donor charges pressed to 1.40 and 1.60 g/cm³ and with transition charges pressed to 0.8, 1.00, and 1.20 g/cm³, using coarse PETN and a 1.28-cm length.

From these successful systems, we have picked the 1.60-g/cm³ donor charge and 1.20-g/cm³ transition charge system for the model study.

III. THE MODEL

The computer model simulates the deflagration-to-detonation transition with a sequence of events beginning with the donor charge prepressurized and with a small region of donor explosive ignited near the hot wire. An ignition front spreads outward at constant velocity with explosive burning behind the ignition front. Then as the donor charge burns, pressure builds in the donor charge and a pressure wave is sent into the PETN transition charge. This pressure wave compacts some of the transition charge and forms a shock, which grows into a detonation wave traveling down the transition tube. No two-phase flow is allowed; that is, the gaseous products do not flow relative to the solids from which they arose. The ignition front is not calculated from convection processes but is imposed as a constant velocity wave, of which the velocity is a model parameter.

Calculations herein were done with the 2DL code,² a two-dimensional, Lagrangian, finite difference, fluid dynamics computer code, using cylindrically symmetric (r,z) geometry. The initial problem SE-setup is shown in Fig. 2; note that only the interior SE-1 detonator assembly with transition tube is included. The steel case and the air gap between the SE-1 and the steel case were omitted because preliminary calculations indicated that detonation or failure to detonate resulted before the brass expanded to close the air gap. Those calculations seem to indicate that the steel case holds the assembly together during the initial stages of pressure buildup in the donor charge, keeping the transition tube from popping out, but not radially confining the assembly. The heavy lines in the setup figure, with one exception, are material bound-

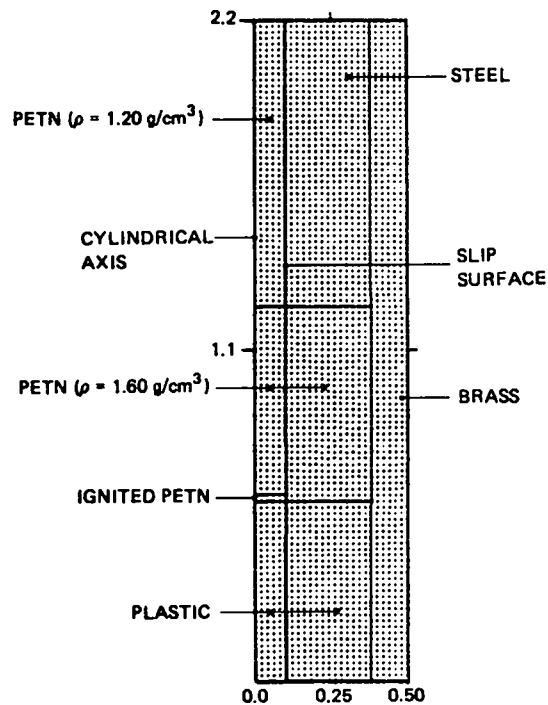


Fig. 2.
SE-1 hot-wire assembly, 2DL problem setup, cylindrical (r,z) geometry.

aries. The exception is the vertical line parallel to the cylindrical axis in the left of the figure. This line is a slip surface that continues throughout the mesh length. The slip surface was included to allow compaction of the low-density PETN ($\rho_0 = 1.20 \text{ g/cm}^3$) in the transition tube. Code restrictions require that a slip surface continue through the entire mesh. The cell mesh is not attached across the slip surface; that is, the inner mesh may move independently of the outer mesh. For this problem set there are no frictional forces at the slip surface.

Dimensions and the numbers of finite difference cells are listed in Table I and shown in Fig. 2 for the initial setup regions. Materials occurring on both sides of the slip surface, for instance, the plastic and the 1.60-g/cm³ PETN, have identical material constants in each region and act as a single material.

In the donor charge burning is allowed and simulated by the simple porous-bed burn model,³ in which the explosive is assumed to be burning on particle surfaces according to the burn surface regression rate law of $\dot{X} = BP^n \text{ (cm/}\mu\text{s)}$ after the passage of an ignition front. The ignition front spreads from already ignited material at a

TABLE I

INITIAL SETUP

Material	Inner Radius (cm)	Outer Radius (cm)	NR Number of Cells	Length (cm)	NZ Number of Cells
(Inside Slip Surface)					
Plastic	0.0	0.1025	5	0.60	30
PETN, $\rho_0 = 1.60 \text{ g/cm}^3$	0.0	0.1025	5	0.02	1
Ignited					
PETN, $\rho_0 = 1.60 \text{ g/cm}^3$	0.0	0.1025	5	0.62	31
Not ignited					
PETN, $\rho_0 = 1.20 \text{ g/cm}^3$	0.0	0.1025	5	0.96	48
Forest Fire					
(Outside Slip Surface)					
Plastic	0.1025	0.38	14	0.60	30
PETN, $\rho_0 = 1.60 \text{ g/cm}^3$	0.1025	0.38	14	0.64	32
Not ignited					
Steel	0.1025	0.38	14	0.96	48
Brass	0.38	0.50	12	2.20	110

constant velocity. Explosive decomposition is described by the equation

$$\frac{dW}{dt} = -\left(\frac{S}{V}\right)_0 W^q B P^n,$$

where

- W = mass fraction of solid explosive,
- $(S/V)_0$ = initial surface-to-volume ratio (1/cm),
- q = particle-geometry-related exponent, and
- P = pressure (Mbar).

The exponent q (in the W^q term) has values of 2/3 for spherical, 1/2 for cylindrical, and 0 for planar particles. The values⁴ of B, n, and q are listed in Table II. The values of $(S/V)_0$ and the ignition velocity were varied in the model parameter study. Initial 0.4-kbar gas pressure is set throughout the donor charge by setting the initial solid-PETN mass fraction there to 0.998. Experimentally, ignition is started with one atmosphere donor charge pressure and pressure increases over a relatively long time. Dinegar has observed delays of a few milliseconds in the functioning of the assemblies. Also, because the mass consumption rate is proportional to pressure and

because pressure should be approximately proportional to the mass fraction of gas products, we expect that the initial pressure growth in time is exponential.

Shock initiation of detonation is allowed in the transition tube and is modeled by the Forest Fire^{3,5} shock-induced reaction rate model, a one-step solid-to-products rate model calculated from the equation of state and experimental shock Hugoniot and Pop plot for the explosive. [The Pop plot is the graph of distance to detonation (run) versus initial shock pressure, as measured in the wedge test, and is named for Alphonse Popolato.⁶] Briefly, the Forest Fire rate is the explosive decomposition rate necessary to accelerate a shock along the time-distance-state space line determined by the Pop plot and Hugoniot, using the Pop plot as a shock growth curve. In the calculations presented here, the rate function is given as a function of local pressure and is used throughout the transition charge; rate function constants are listed in Table II.

The HOM⁷ equation of state is used throughout this calculation. This equation of state represents solids by a Grüneisen expansion off the shock Hugoniot with temperatures calculated by the Walsh and Christian⁸ technique. The gas products are represented by a beta

TABLE II 2DL INPUT CONSTANTS

Porous-bed burn constants for PETN, where $\rho_0 = 1.60 \text{ g/cm}^3$.

$$\frac{dW}{dt} = -\left(\frac{S}{V}\right)_0 W^q B P^n \left(\frac{1}{\mu s}\right),$$

where $q = 0.667$, $B = 0.0119$, and $n = 1.0$, with $P = \text{Mbar}$.

HOM CONSTANTS - PETN, RHO = +1.20

```
+0.01272      +2.3      +0.      +0.
+0.      +7.35770705112E+00+2.39083797487E+01+1.16201137629E+02
+1.96236668634E+02+1.16157063364E+02+1.15      +0.24
+8.3333333333E-01+0.000232      +0.      +0.
+330.430499777      +0.000001      +0.      +0.
+0.      +0.      +0.
-3.17802221190E+00-2.35331643478E+00+2.17043373808E-01+1.17479938619E-02
-5.94101012630E-03-1.42326845168E+00+4.77286576745E-01+6.03149941862E-02
+4.05801307902E-03+1.08173212997E-04+7.93913046699E+00-4.31173734538E-01
+1.03363956902E-01-2.32720523000E-02+2.12830586356E-03+0.5
+0.1
```

FOREST FIRE POLYNOMIAL COEFFICIENTS

```
15      PETN, RHO=1.20, ESTIMATED POP PLOT AND HUGONIOT, BKW GAS
1.440000000000E-01 2.000000000000E-03 DW/DT=-W**F(P)
-1.22090225473E+18 1.37845714582E+18-6.99723707168E+17 2.10990512254E+17
-4.20660384487E+16 5.84118991286E+15-5.79662003909E+14 4.15224044246E+13
-2.14323058755E+12 7.87550287132E+10-2.01421458481E+09 3.46783232499E+07
-3.86339277739E+05 2.80914048267E+03-1.23187022045E+01
```

=====

HOM CONSTANTS - STEEL, RHO = +7.917

```
+4.58      -001+1.51      +000+0.      +0.
+0.      -3.82382587453+003-7.03211954024+003-4.82670213894+003
-1.46678402118+003-1.66391615983+002+2.02      +1.07      -001
+1.26310471138-001+1.17      -005+0.      +0.
+300.      +0.000001      +0.      +0.
+0.      +0.      +0.
```

=====

HOM CONSTANTS - BRASS, RHO = +8.413

```
+0.3762      +1.434      +0.      +0.
+0.      -1.82751495953E+03-3.29082347949E+03-2.20477399694E+03
-6.52697187349E+02-7.19406164970E+01+2.314      +0.09
+1.18863663378E-01+0.000020533      +0.      +0.
+300.      +0.000001      +0.      +0.
+0.      +0.      +0.
```

=====

HOM CONSTANTS - PLASTIC, RHO = +1.18

```
+0.2432      +000+1.5785      +000+1.0      -004+0.0      +000
+0.0      +000+5.29380243506+000-4.24950371368+000-1.55055576332+001
-3.08638075572+001-1.46708193739+001+1.0      +000+0.35      +000
+8.47457627      -001+1.0      -004+0.      +0.
+3.0      +002+1.0      -006+0.0      +0.0
+0.      +0.      +0.
```

=====

HOM CONSTANTS - PETN, RHO = +1.60

```
+0.1422      +2.3      +0.      +0.
+0.      +1.67014104114E+01+8.22635996514E+01+2.16390936772E+02
+2.41187353514E+02+1.00842072079E+02+1.15      +0.24
+0.625      +0.000232      +0.      +0.
+304.376342781      +0.000001      +0.      +0.
+0.      +0.      +0.
-3.38506732351E+00-2.43076581504E+00+2.39523413339E-01-6.95482728581E-04
-3.39665423195E-03-1.55478794487E+00+4.76859124482E-01+5.29479003308E-02
+2.49895318274E-03+2.41827550727E-05+7.62534466015E+00-5.08360905427E-01
+7.53979259123E-02+2.52285533703E-02-8.00310612005E-03+0.5
+0.1
```

FOREST FIRE POLYNOMIAL COEFFICIENTS

```
13      PETN, RHO=1.60, PCJ=0.2564, DCJ=0.7818, VCJ=0.46118
2.56326000000E-01+0.003      DW/DT=-W**F(P)
-1.45372719700E+13 2.13878630671E+13-1.39169518661E+13 5.27427850939E+12
-1.29042984524E+12 2.13542626252E+11-2.43534878228E+10 1.91547535104E+09
-1.02479283910E+08 3.63112108861E+06-8.24093189751E+04 1.22282347454E+03
-1.08522971453E+01
```

expansion off the BKW^{9,10} calculated detonation isentrope. Solid and gas product mixtures are calculated by simultaneous solution of the solid and gas equations for pressure and temperature equilibrium, assuming ideal volume and energy partition according to mass fraction. The HOM constants for each material are listed in Table II.

Because Forest Fire depends upon the shock Hugoniot and Pop plot, and HOM depends upon the shock Hugoniot for the solid equation of state, these relations must be known for each material in the model to which they apply. Experimental data are available except for PETN with density $\rho_0 = 1.20 \text{ g/cm}^3$, where

the Pop plot and Hugoniot need to be estimated. These estimates are made and the method for each is presented below. Experimental wedge data on PETN at other densities¹¹⁻¹³ are used heavily.

The Pop plot for $\rho_0 = 1.20 \text{ g/cm}^3$ PETN is estimated by a line parallel to the $\rho_0 = 1.40 \text{ g/cm}^3$ PETN Pop plot. We found this approach reasonable by inspection of the various PETN Pop plots in Fig. 3. [The least-square linear $\ln(\text{run}) = a + b \ln(P)$ fits are listed in Table III.] By paralleling the $\rho_0 = 1.40 \text{ g/cm}^3$ line, it is sufficient to estimate only one point on the line. Again looking at the Pop plot in Fig. 3, a 0.3-cm distance to detonation lies interior to the data range for each of the data sets and

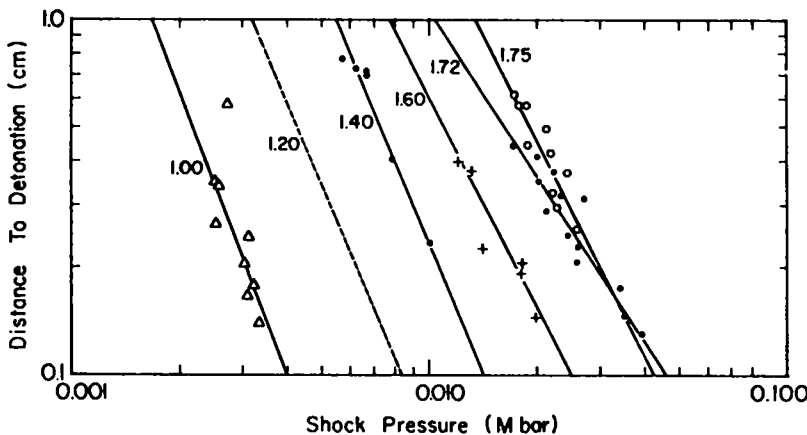


Fig. 3. Distance to detonation as a shock pressure function at various densities, (g/cm^3). The 1.20- g/cm^3 line is estimated from the wedge test data.

TABLE III

PETN POP PLOTS—
LEAST-SQUARE FITS FROM WEDGE DATA

$\ln(\text{run}) = a + b \ln(P)$, where
run = distance to detonation (cm), and
P = initial shock pressure (Mbar).
(P* = shock pressure for run = 0.3 cm.)

Initial Density, ρ_0 (g/cm^3)	Constants		Shock Pressure, P* (Mbar)
	a	b	
1.00	-16.76803	-2.62043	0.00263
1.40	-12.42600	-2.38626	0.00907
1.60	-9.44241	-1.94113	0.01435
1.72	-7.10742	-1.55638	0.02253
1.75	-8.64881	-2.00592	0.2444
	Estimated Pop Plot		
1.20	-13.78	-2.40	0.0053

serves as the distance to detonation for the unknown point, with the corresponding pressure to be determined.

The pressure is determined from a graph of the pressure required for a 0.3-cm run from each of the Pop plot lines as a density function in log-log coordinates in Fig. 4. The points define the solid line at $\rho_0 = 1.40$ and 1.60 g/cm^3 , which gives a shock pressure of 0.053 Mbar for $\rho_0 = 1.20 \text{ g/cm}^3$. Note that the point for $\rho_0 = 1.00 \text{ g/cm}^3$ lies nearly on the line. The Pop plot so estimated is then $\ln(\text{run}) = -13.78 - 2.40 \ln(P)$ with run = cm and $P = \text{Mbar}$.

The shock Hugoniot line ($U_s = C + SU_p$) is estimated from a uniform Hugoniot representation for each of the densities by fitting each of the (U_p, U_s) data sets to a straight line with slope 2.3, letting the intercept at $U_p = 0$ fall where it may (see Fig. 5 and Table IV). These intercepts are plotted as a density function; in particular, the intercepts are graphed against ρ_{max}/ρ_0 in log-log coordinates in Fig. 6. The motivation for this method came from an observation on the PETN data at the extremes of the density range. First, Olinger and Cady¹⁴ gave a Hugoniot for 1.774-g/cm^3 PETN derived from x-ray diffraction patterns taken at pressures up to 0.100 Mbar. Their quadratic Hugoniot relation is well approx-

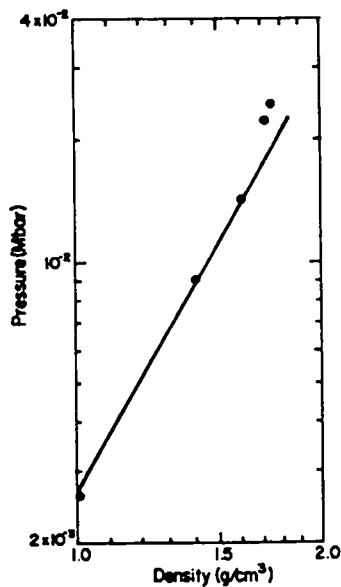


Fig. 4.

Shock pressure needed for a 0.3-cm distance to detonation as a function of PETN density. The solid line is drawn through the 1.40 and 1.60 g/cm^3 points.

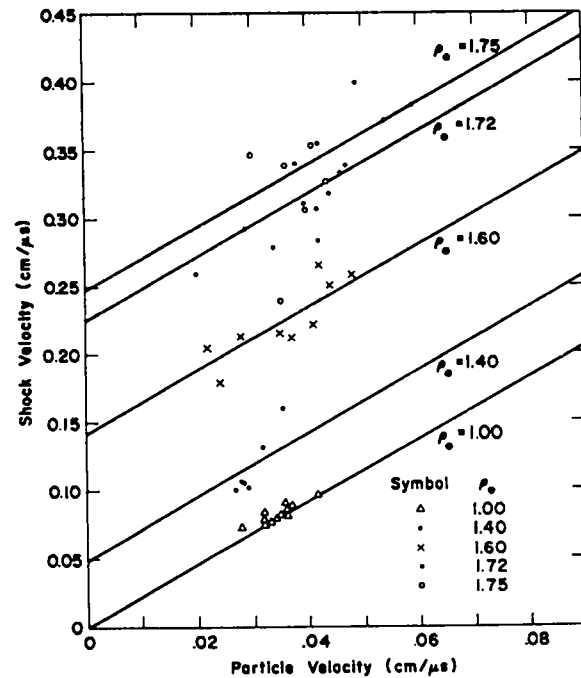


Fig. 5.

PETN shock Hugoniots. Data points are from Los Alamos group WX-2 wedge tests. Lines are least-squares fits with constant slope of 2.3. Labels on each line indicate the density (g/cm^3).

TABLE IV

SHOCK HUGONIOT INTERCEPTS
FOR CONSTANT SLOPE
 $U_s = C_0 + 2.3 U_p$ LINES

Initial Density,		C_0	Fit C_0
ρ_0 (g/cm^3)	ρ_{max}/ρ_0	($\text{cm}/\mu\text{s}$)	($\text{cm}/\mu\text{s}$)
1.75	1.01600	0.2469	0.2526
1.72	1.03372	0.2254	0.2254
1.60	1.11125	0.1422	0.1371
1.40	1.27000	0.0488	0.0495
1.00	1.778	0.0033	0.0019

imated by the linear relation $U_s = 0.232 + 2.306 U_p$ ($\text{cm}/\mu\text{s}$). Secondly, the data Seay and Seely¹² gave for 1.00 g/cm^3 PETN is well fit by the line $U_s = 2.3 U_p$, if the shock velocities are corrected by a factor of 0.9. (The velocities were estimated to be 10% too high because the velocities reported were average velocities over the entire run to detonation and not initial velocities.)

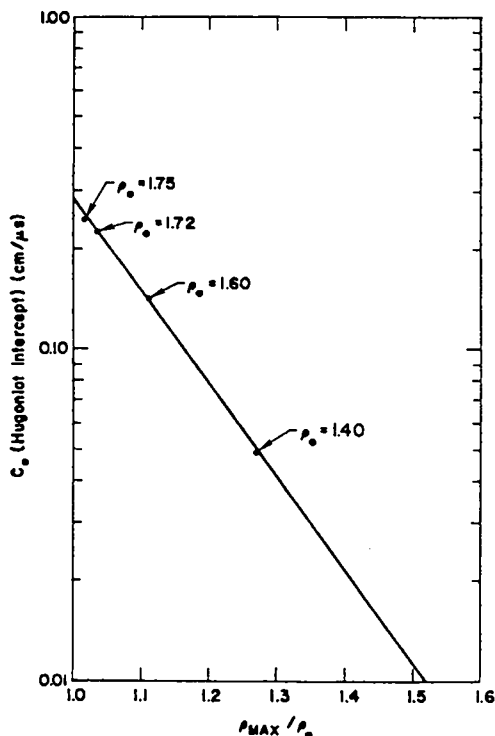


Fig. 6.
PETN constant slope Hugoniot intercepts as a density function. Labels at the points indicate density (g/cm³).

The least-squares fit of the intercepts as a density function is $C = \beta_1 \exp(-\beta_2 \rho_{\max} / \rho_0)$, where $\rho_{\max} = 1.778$ g/cm³, $\beta_1 = 171.60519$ (cm/ μ s), and $\beta_2 = 6.41846$, with a coefficient determination $r^2 = 0.9988$. Evaluation of the fit at $\rho_0 = 1.20$ g/cm³ gives the Hugoniot relation $U_s = 0.0127 + 2.3 U_p$. Note also that evaluation at $\rho_0 = 1.00$ g/cm³ gives an intercept of $C_0 = 0.0033$ cm/ μ s.

The Forest Fire rate calculation based on these estimates is listed in Table V.

IV. CALCULATION SETS

For each of the three ignition velocities—0.05, 0.10, and 0.20 cm/ μ s—a calculation was made for various surface-to-volume ratios in the porous-bed burn model. Graphic 2DL output is shown in Figs. 7a-7d, 8a-8f, and 9a-9d, with the ignition velocity held constant in each set. The ignition front position is independent of the surface-to-volume ratio, is thus the same in time for each set calculation, and so is plotted only once for each set. Sequential pressure contours are presented for each calculation with mass fraction contours included for

those times showing reaction progress. Table VI lists the figure numbers.

At the bottom of each pressure contour frame are listed the time (μ s) from the beginning of the calculation, the pressure contour interval ($\Delta P =$ kbar), and the maximum pressure ($P_{\max} =$ kbar) over all cells. At the bottom of the mass fraction plots are listed the time and mass fraction contour interval (ΔW), and at the bottom of the ignition front position plot is listed the time only.

In examining the pressure plot sequences, the pressure contour interval and the maximum pressure should be noted carefully. The contour interval is varied to limit the number of contour lines so a rapid increase in pressure (say a doubling) from one frame to the next may not be apparent from contour lines because the interval may also increase and the number of lines would stay about constant.

V. CONCLUSIONS

Figure 10 shows general features of the model calculations as a graph of the maximum pressure taken from the entire mesh plotted as a function of ignition time. The calculation set with 0.05-cm/ μ s ignition velocity shows steady pressure increase until 12 μ s, followed by a decrease in pressure. The maximum in the curve occurs soon after the arrival of the ignition front at the top of the donor charge, see Fig. 7a. Apparently, the reason for the pressure drop is that the brass case expands faster than gas is evolved to fill the increased volume; the long time required to get the entire mass burning allows for greater acceleration of the brass, see Figs. 7b and 7d. The calculation set with 0.1-cm/ μ s ignition velocity shows a maximum in the pressure-time curve in Fig. 10 for surface-to-volume ratios of 400 and 500/cm, but steady pressure increase for (S/V) of 600 and 800/cm. The line for (S/V) = 500/cm appears to decrease but surely must induce shock initiation into the PETN transition charge because the pressure is high enough. Again, the drop is due to case expansion before shock-induced decomposition in the transition charge has proceeded very far. The calculation set for 0.2-cm/ μ s ignition velocity shows similar behavior with shorter times. The overall behavior is simply stated—the transition to detonation is achieved most rapidly where a high mass burn rate occurs in compacted explosive. Slow ignition delays the gas production and allows greater expansion, and thus gives lower density in the burning bed.

TABLE V

FOREST FIRE CALCULATION FOR PETN

$$\rho_0 = 1.20 \text{ g/cm}^3$$

INPUT

PETN, RHO=1.20, ESTIMATED POP PLOT AND HUGONIOT, BKW GAS 28JAN81 RHO = 1.20000

POP PLOT, LN(RUN) = A1 + A2*LN(P-A3), A1 = -1.378000E+01 A2 = -2.400000E+00 A3 = 0.

REACTION HUGONIOT, US = C + S*UP, C = 1.300000E-02 S = 2.400000E+00

CJ DETONATION PRESSURE = 1.440000E-01

HOM EQUATION OF STATE CONSTANTS

PETN, RHO=1.20, US=C+2.3*UP

UNREACTED EXPLOSIVE

1.27200000000E-02	2.30000000000E+00	0.	0.
0.	7.35770705112E+00	2.39083797487E+01	1.16201137629E+02
1.96236668634E+02	1.16157063364E+02	1.15000000000E+00	2.40000000000E-01
8.33333333333E-01	2.32000000000E-04	0.	0.
3.30430499777E+02	1.00000000000E-06	0.	0.
0.	0.	0.	0.

DETONATION PRODUCTS

-3.17802221190E+00	-2.35331643478E+00	2.17043373808E-01	1.17479938619E-02
-5.94101012630E-03	-1.42326845168E+00	4.77286576745E-01	6.03149941862E-02
4.05801307902E-03	1.08173212997E-04	7.93913046699E+00	-4.31173734538E-01
1.03363956902E-01	-2.32720523000E-02	2.12830586356E-03	5.00000000000E-01
1.00000000000E-01			

RATE CALCULATION

PETN, RHO=1.20, ESTIMATED POP PLOT AND HUGONIOT, BKW GAS 28JAN81 RHO = 1.20000
 POP PLOT, LN(RUN) = A1 + A2*LN(P-A3), A1 = -1.378000E+01 A2 = -2.400000E+00 A3 = 0.
 REACTION HUGONIOT, US = C + S*UP, C = 1.300000E-02 S = 2.400000E+00

RUN	P	V	UP	US	W	RATE	TEMPERATURE	TIME
3.11136	.00200	.55052	.02378	.07008	.99798	3.2821E-04	1940.74673	37.30366
1.17579	.00300	.53970	.02968	.08423	.99704	1.4281E-03	2167.38762	11.69599
.58949	.00400	.53304	.03466	.09618	.99619	4.2872E-03	2352.62863	5.12700
.34506	.00500	.52841	.03905	.10671	.99541	9.5762E-03	2509.69256	2.70183
.22277	.00600	.52494	.04302	.11624	.99470	1.8400E-02	2645.70169	1.60001
.15388	.00700	.52222	.04667	.12500	.99403	3.1723E-02	2765.32529	1.02708
.11169	.00800	.52001	.05007	.13316	.99341	5.0748E-02	2871.73669	.69942
.08419	.00900	.51817	.05326	.14082	.99281	7.6711E-02	2967.30797	.49829
.06538	.01000	.51660	.05628	.14807	.99224	1.1093E-01	3053.83397	.36788
.01239	.02000	.50796	.08067	.20661	.98723	1.2626E+00	3627.22341	.04985
.00468	.03000	.50406	.09939	.25154	.98275	5.3560E+00	3945.06772	.01546
.00235	.04000	.50171	.11517	.28942	.97834	1.5310E+01	4152.41174	.00673
.00137	.05000	.50009	.12908	.32279	.97384	3.5276E+01	4299.00335	.00353
.00089	.06000	.49890	.14165	.35297	.96915	7.1076E+01	4407.52541	.00208
.00061	.07000	.49797	.15322	.38072	.96417	1.3055E+02	4490.09934	.00133
.00044	.08000	.49721	.16398	.40655	.95884	2.2406E+02	4553.89792	.00091
.00034	.09000	.49659	.17409	.43081	.95305	3.6660E+02	4603.45182	.00064
.00026	.10000	.49606	.18365	.45376	.94673	5.7395E+02	4641.85274	.00048
.00021	.11000	.49560	.19274	.47559	.93974	8.7958E+02	4671.13319	.00036
.00017	.12000	.49520	.20143	.49644	.93195	1.3136E+03	4692.81022	.00028
.00014	.13000	.49485	.20977	.51644	.92319	1.9332E+03	4707.90640	.00022
.00012	.14000	.49454	.21779	.53569	.91323	2.7897E+03	4717.23571	.00018
.00010	.15000	.49426	.22553	.55426	.90177	4.0289E+03	4721.21584	.00015
.00008	.16000	.49400	.23301	.57222	.88839	5.7604E+03	4720.16041	.00012

POLYNOMIAL FIT

PETN, RHO=1.20, ESTIMATED POP PLOT AND HUGONIOT, BKW GAS 28JAN81 RHO = 1.20000
 LN(RATE) = C(1) + C(2)**P + ... + C(M+1)**(P**M)
 C(I=1,15) = -1.2318702205E+01 2.8091404827E+03 -3.8633927774E+05 3.4678323250E+07 -2.0142145848E+09
 7.8755028713E+10 -2.1432305875E+12 4.1522404425E+13 -5.7966200391E+14 5.8411899129E+15
 -4.2066038449E+16 2.1099051225E+17 -6.9972370717E+17 1.3784571458E+18 -1.2209022547E+18

PRESSURE	RATE	FIT	REL. ERROR
2.000000E-03	3.282067E-04	3.360700E-04	-.023959
3.000000E-03	1.428149E-03	1.391311E-03	.025794
4.000000E-03	4.287172E-03	4.139068E-03	.034546
5.000000E-03	9.576162E-03	9.658418E-03	-.008590
6.000000E-03	1.839967E-02	1.889484E-02	-.026911
7.000000E-03	3.172286E-02	3.257393E-02	-.026828
8.000000E-03	5.074789E-02	5.133875E-02	-.011643
9.000000E-03	7.671084E-02	7.596307E-02	.009748
1.000000E-02	1.109302E-01	1.075202E-01	.030740
2.000000E-02	1.262566E+00	1.270871E+00	-.006578
3.000000E-02	5.355952E+00	5.374420E+00	-.003448
4.000000E-02	1.531000E+01	1.510351E+01	.013487
5.000000E-02	3.527619E+01	3.586095E+01	-.016577
6.000000E-02	7.107579E+01	7.059710E+01	.006735
7.000000E-02	1.305465E+02	1.294960E+02	.008047
8.000000E-02	2.240611E+02	2.271405E+02	-.013744
9.000000E-02	3.665977E+02	3.646305E+02	.005366
1.000000E-01	5.739454E+02	5.700362E+02	.006811
1.100000E-01	8.795843E+02	8.902111E+02	-.012082
1.200000E-01	1.313577E+03	1.301449E+03	.009233
1.300000E-01	1.933248E+03	1.941716E+03	-.004380
1.400000E-01	2.789713E+03	2.786098E+03	.001296
1.500000E-01	4.028898E+03	4.029805E+03	-.000225
1.600000E-01	5.760421E+03	5.760335E+03	.000015

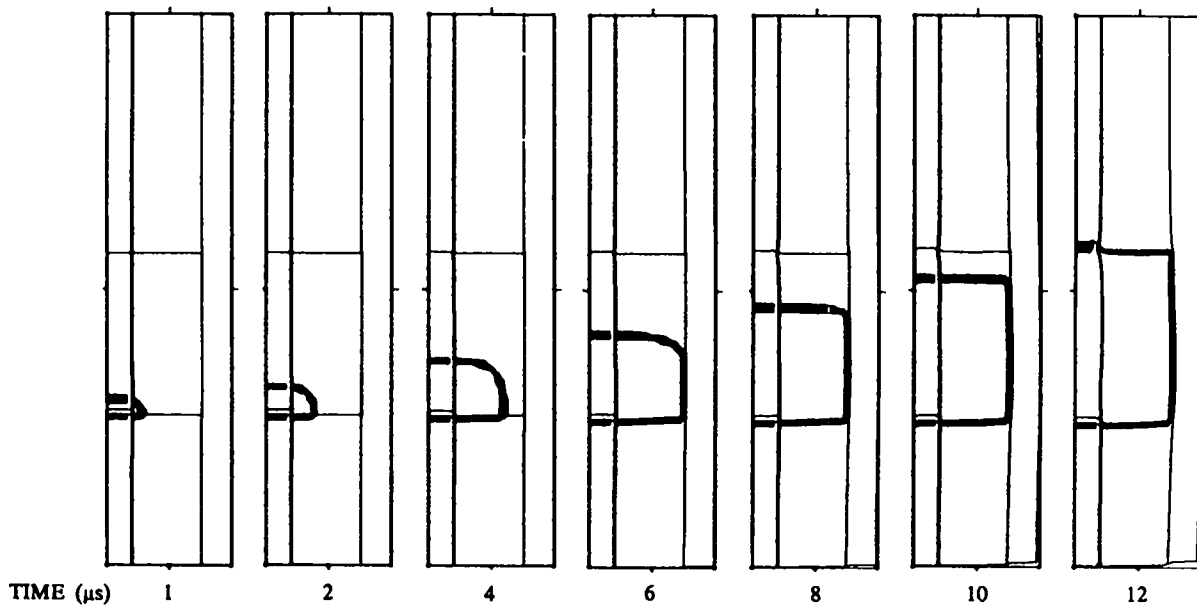


Fig. 7a.

Ignition front position. Ignition velocity = $0.05 \text{ cm}/\mu\text{s}$. Burning occurs behind the ignition front.

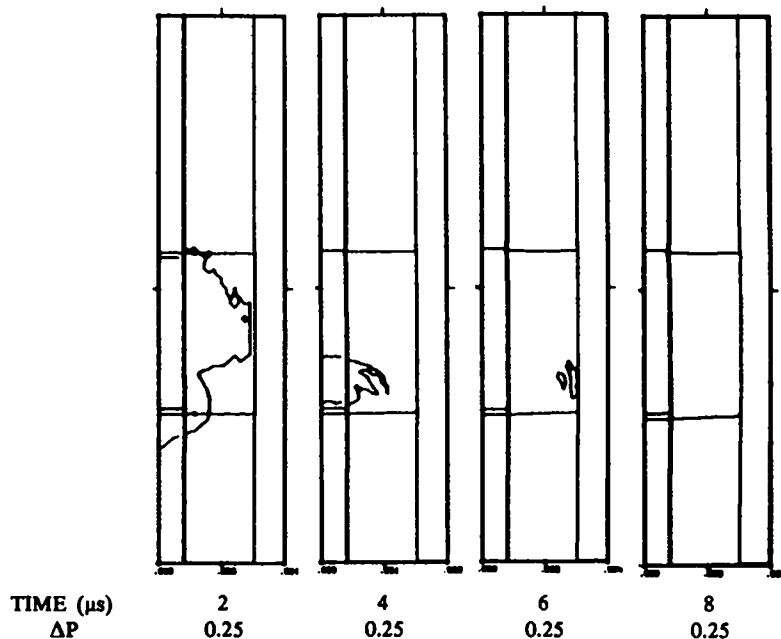
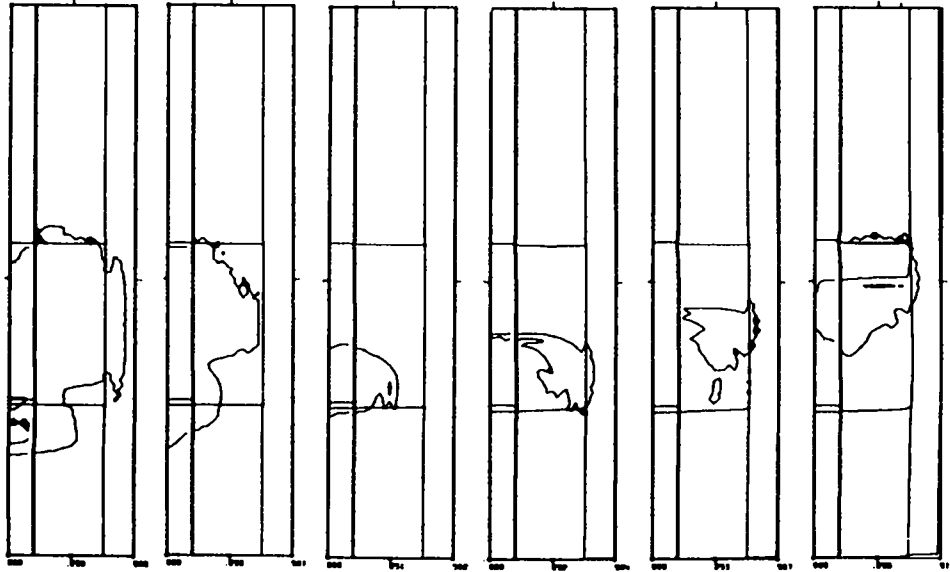


Fig. 7b.

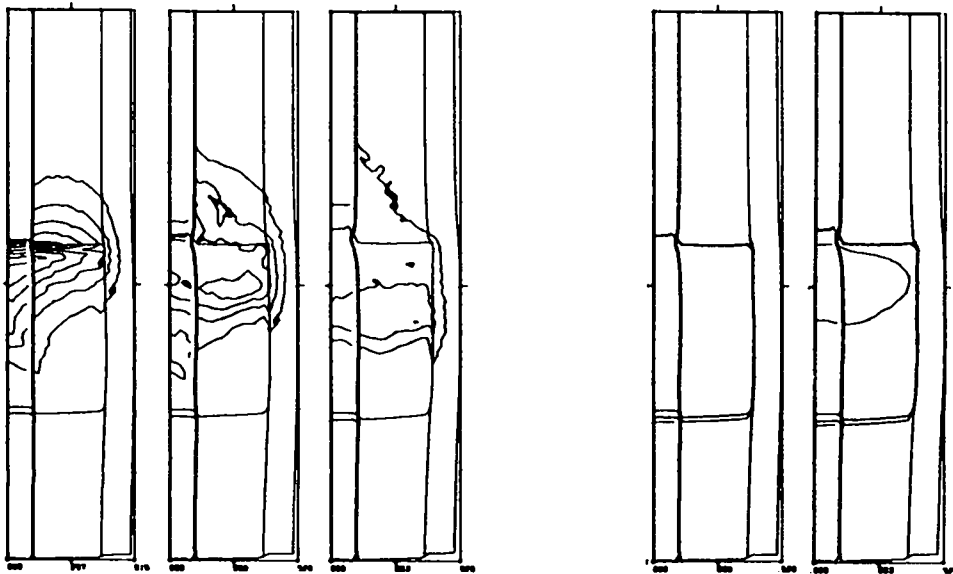
Pressure contours. Ignition velocity = $0.05 \text{ cm}/\mu\text{s}$ and $(S/V)_0 = 400/\text{cm}$. $\Delta P =$ contour interval (kbar).



TIME (μ s)	1	2	4	6	8	10
ΔP	0.25	0.25	0.25	0.25	0.25	0.25
P_{max}	---	---	---	---	---	0.54

Fig. 7c.

Pressure contours. Ignition velocity = 0.05 cm/ μ s and $(S/V)_0 = 500/cm$. ΔP = contour interval (kbar). P_{max} = maximum pressure (kbar).



TIME (μ s)	12	14	16	TIME (μ s)	14	16
ΔP	0.25	0.25	0.25	ΔW	0.025	0.025
P_{max}	1.61	1.14	0.76			

Pressure (P) contours

Mass fraction (W) contours

Fig. 7c. (cont)

Ignition velocity = 0.05 cm/ μ s and $(S/V)_0 = 500/cm$. ΔW = contour interval fraction. ΔP = contour interval (kbar). P_{max} = maximum pressure (kbar).

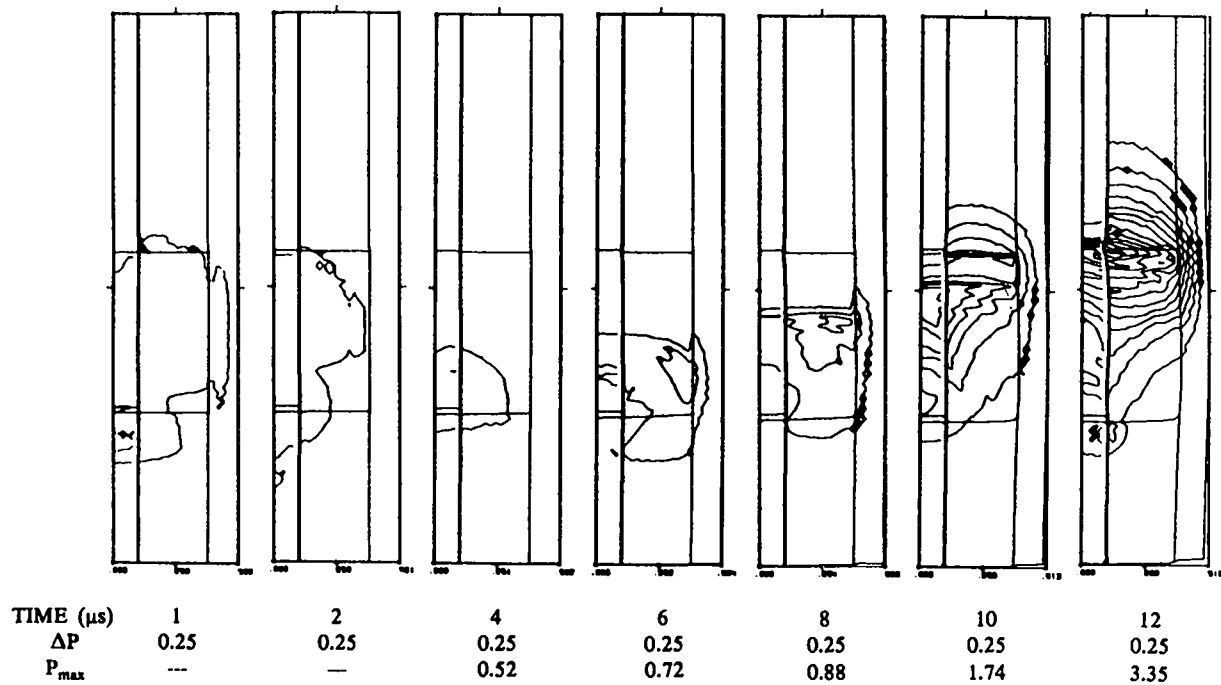


Fig. 7d.

Pressure contours. Ignition velocity = $0.05 \text{ cm}/\mu\text{s}$ and $(S/V)_0 = 600/\text{cm}$. ΔP = contour interval (kbar). P_{max} = maximum pressure (kbar).

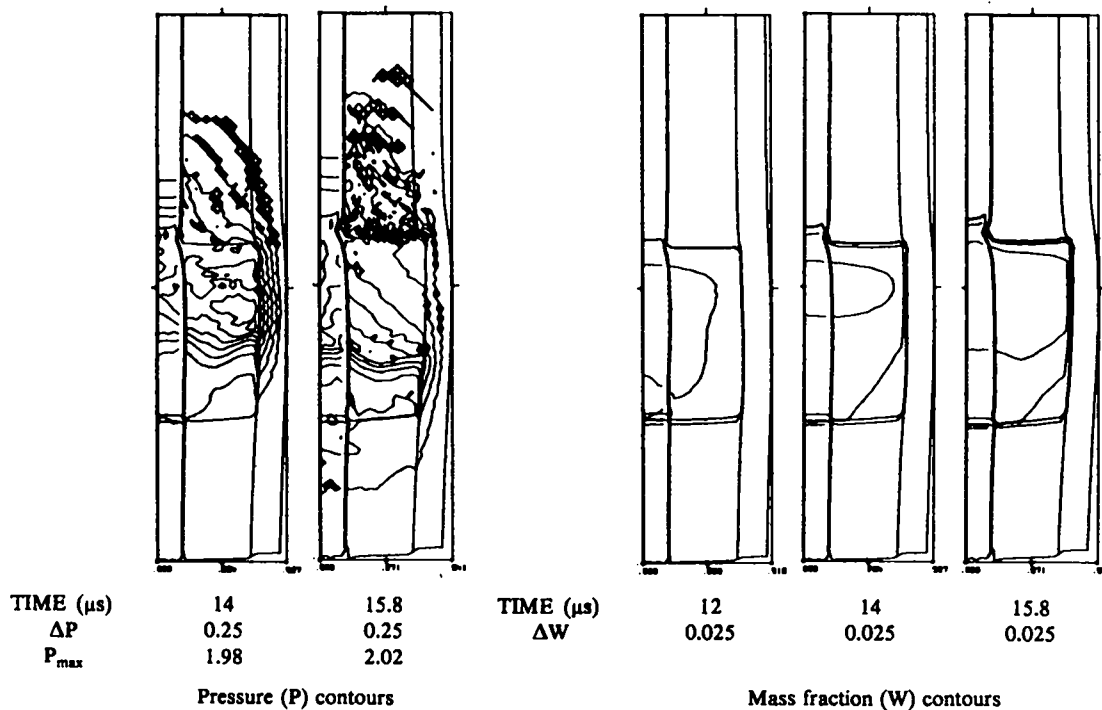


Fig. 7d. (cont)

Ignition velocity = $0.05 \text{ cm}/\mu\text{s}$ and $(S/V)_0 = 600/\text{cm}$. ΔW = contour interval fraction. ΔP = contour interval (kbar). P_{max} = maximum pressure (kbar).

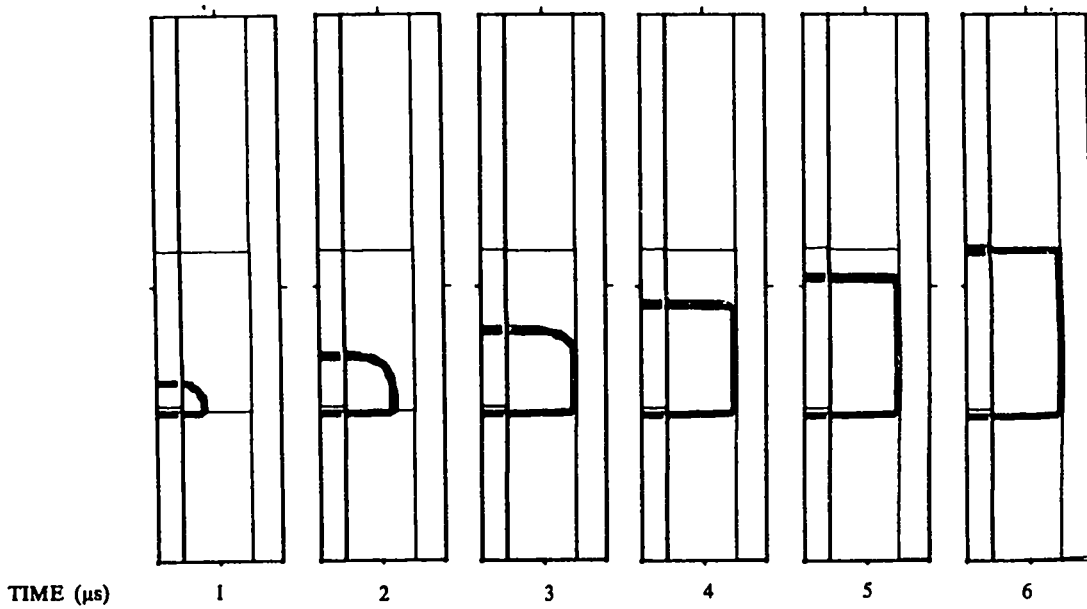


Fig. 8a.
 Ignition front position. Ignition velocity = $0.10 \text{ cm}/\mu\text{s}$. Burning occurs behind the ignition front.

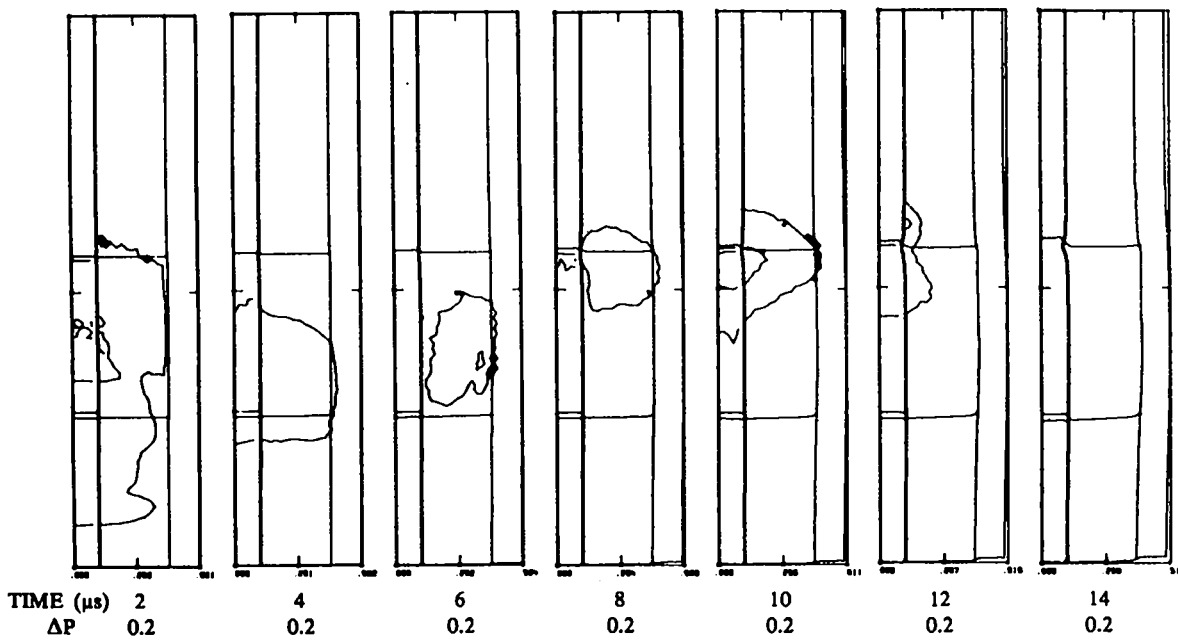


Fig. 8b.
 Pressure contours. Ignition velocity = $0.10 \text{ cm}/\mu\text{s}$ and $(S/V)_0 = 200/\text{cm}$. ΔP = contour interval (kbar).

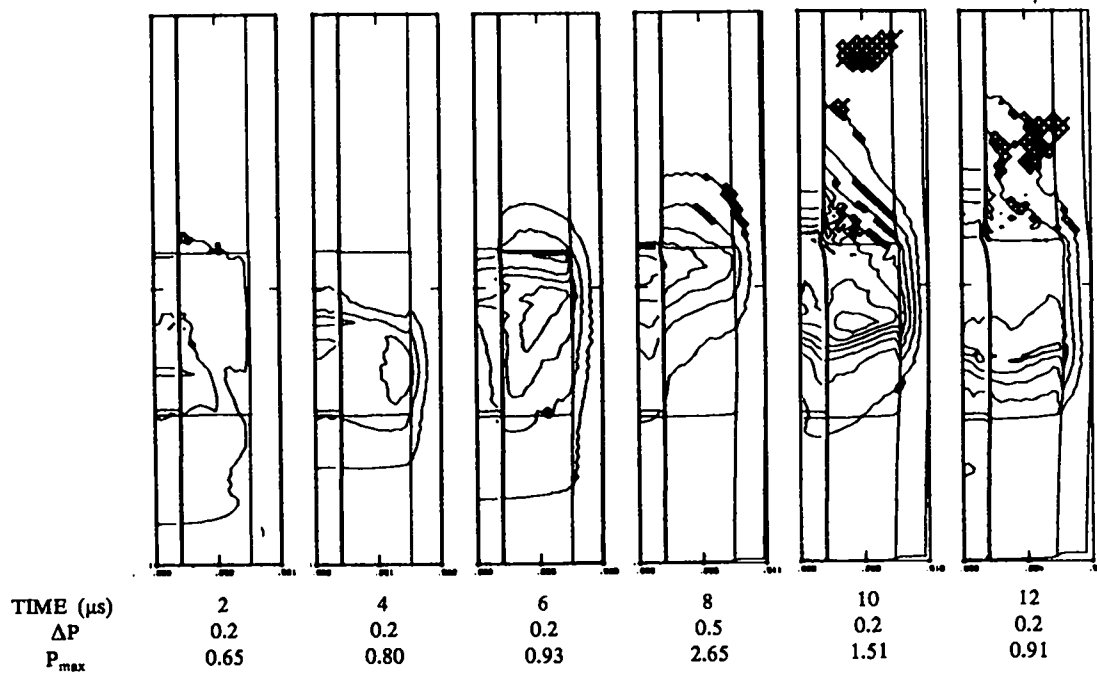


Fig. 8c.
 Pressure contours. Ignition velocity = 0.10 cm/ μs and $(S/V)_0 = 400/\text{cm}$. ΔP = contour interval (kbar).
 P_{max} = maximum pressure (kbar).

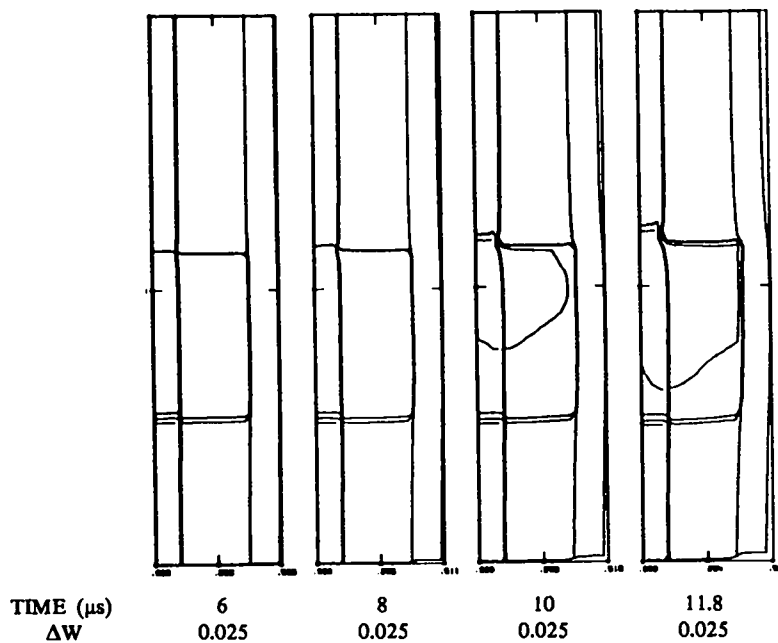


Fig. 8c. (cont)
 Mass fraction (W) contours. Ignition velocity = 0.10 cm/ μs and
 $(S/V)_0 = 400/\text{cm}$. ΔW = contour interval fraction.

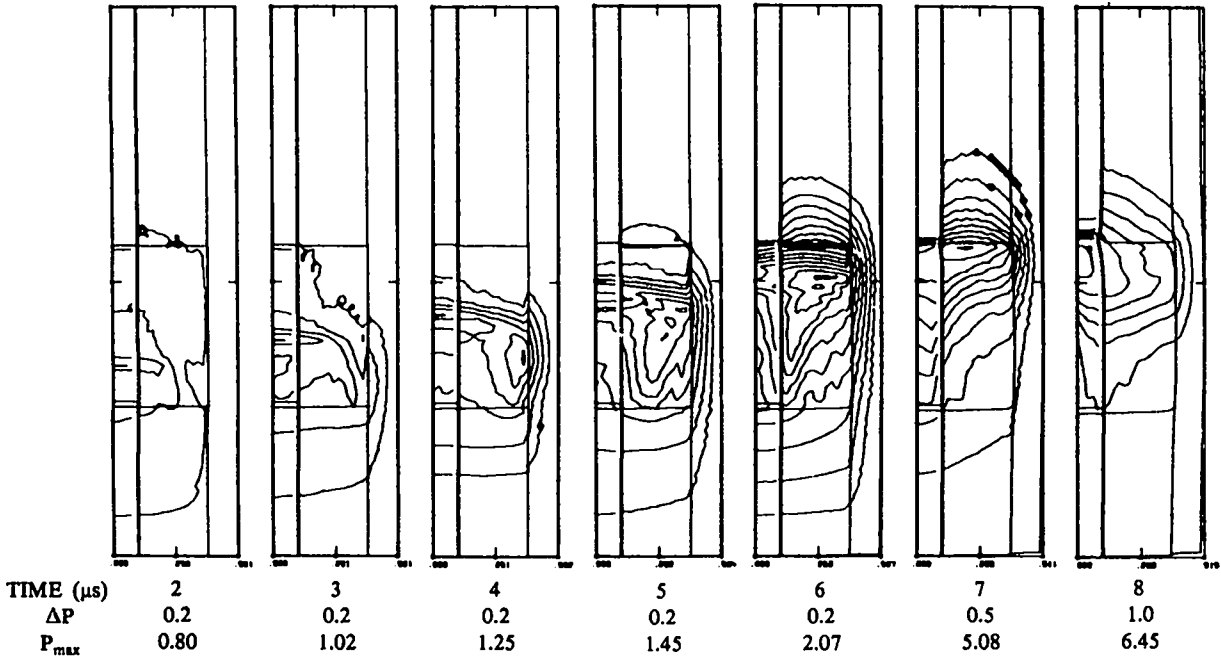


Fig. 8d.
 Pressure contours. Ignition velocity = 0.10 cm/ μ s and $(S/V)_0 = 500$ /cm. ΔP = contour interval (kbar). P_{\max} = maximum pressure (kbar).

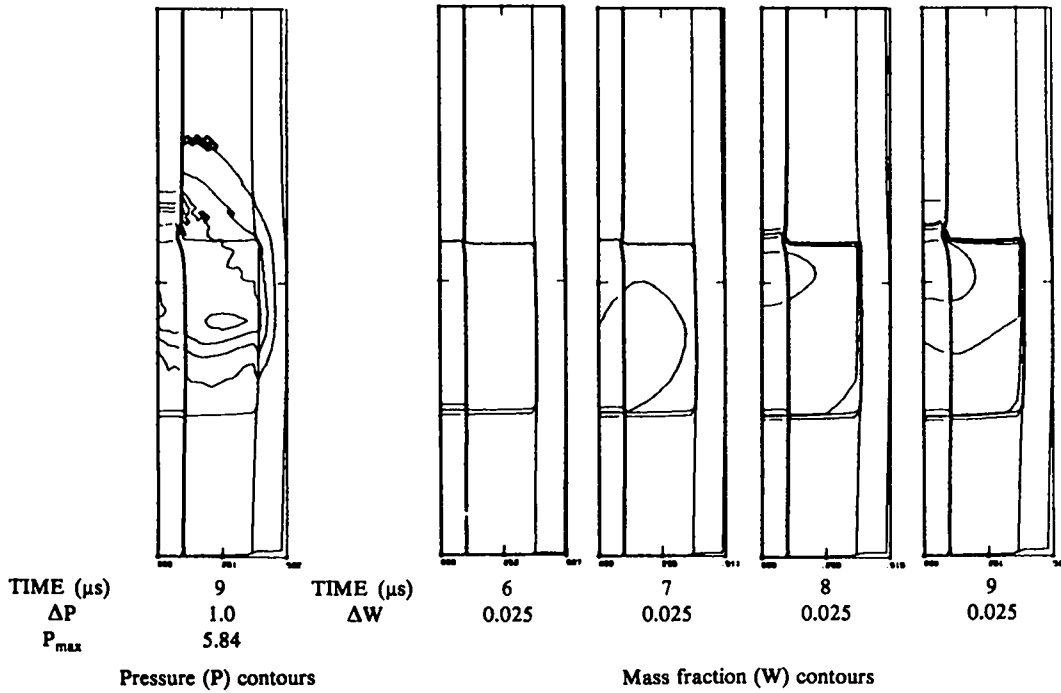


Fig. 8d. (cont)
 Ignition velocity = 0.10 cm/ μ s and $(S/V)_0 = 500$ /cm. ΔP = contour interval (kbar). ΔW = contour interval fraction. P_{\max} = maximum pressure (kbar).

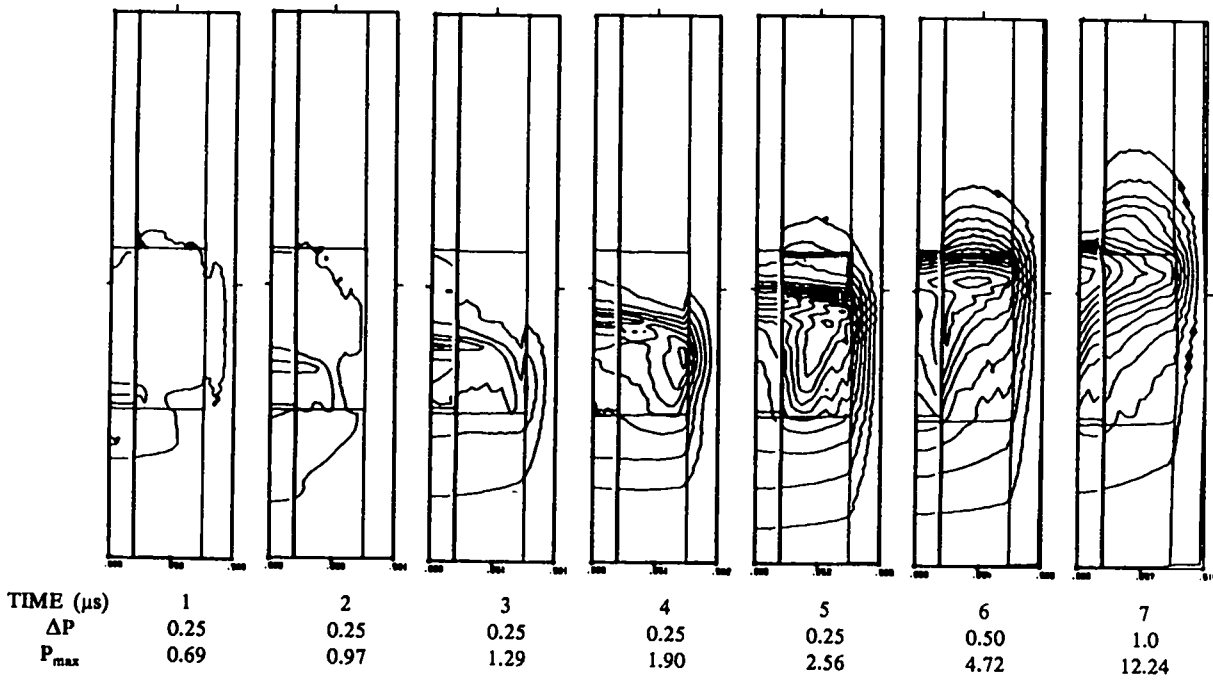


Fig. 8e.
 Pressure contours. Ignition velocity = 0.10 cm/ μ s and $(S/V)_0 = 600$ /cm. ΔP = contour interval (kbar). P_{max} = maximum pressure (kbar).

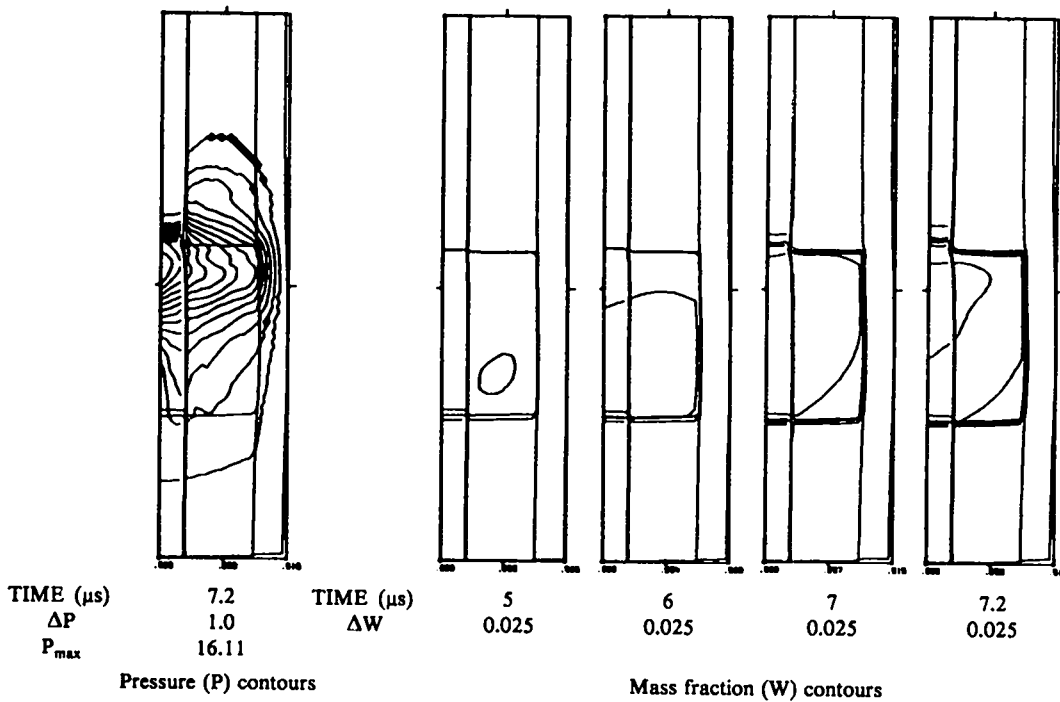


Fig. 8e. (cont)
 Ignition velocity = 0.10 cm/ μ s and $(S/V)_0 = 600$ /cm. ΔP = contour interval (kbar). ΔW = contour interval fraction. P_{max} = maximum pressure (kbar).

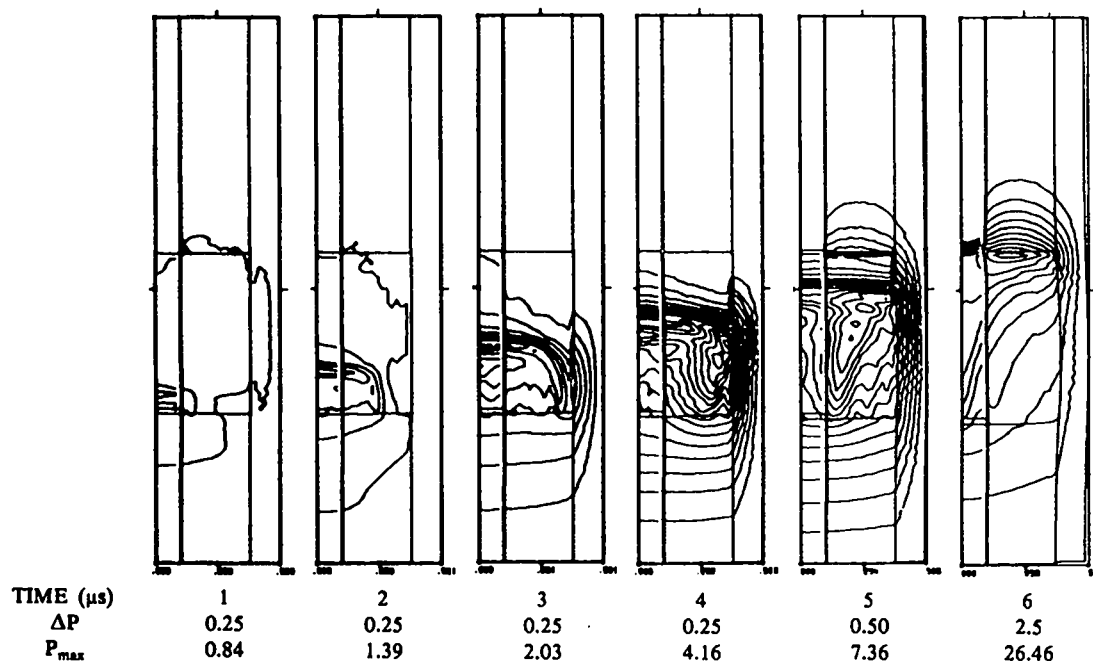


Fig. 8f.

Pressure contours. Ignition velocity = 0.10 cm/ μs and $(S/V)_0 = 800/\text{cm}$. ΔP = contour interval (kbar). P_{max} = maximum pressure (kbar).

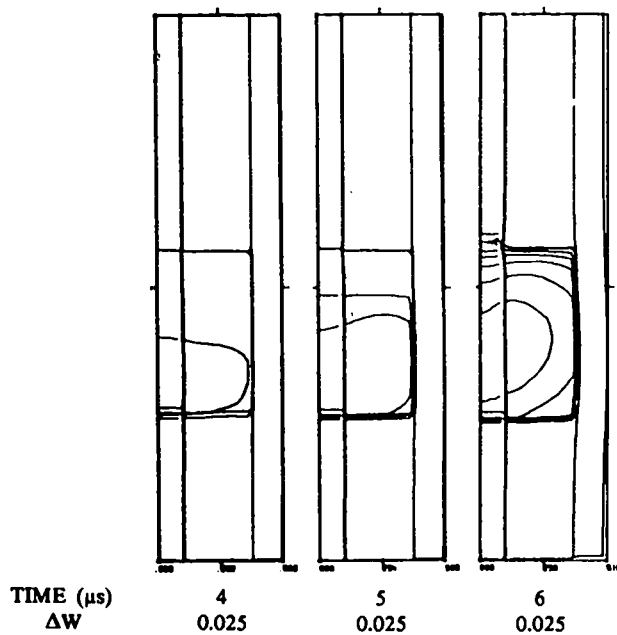


Fig. 8f. (cont)

Mass fraction (W) contours. Ignition velocity = 0.10 cm/ μs and $(S/V)_0 = 800/\text{cm}$. ΔW = contour interval fraction.

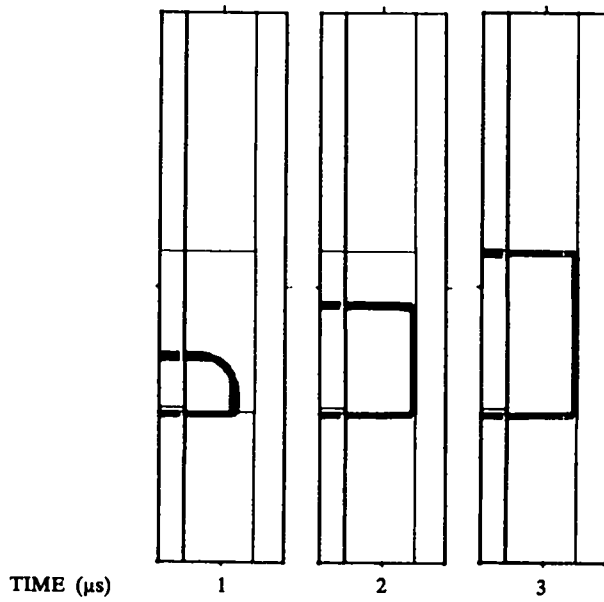


Fig. 9a.
 Ignition front position. Ignition velocity = 0.20 cm/ μs .
 Burning occurs behind the ignition front.

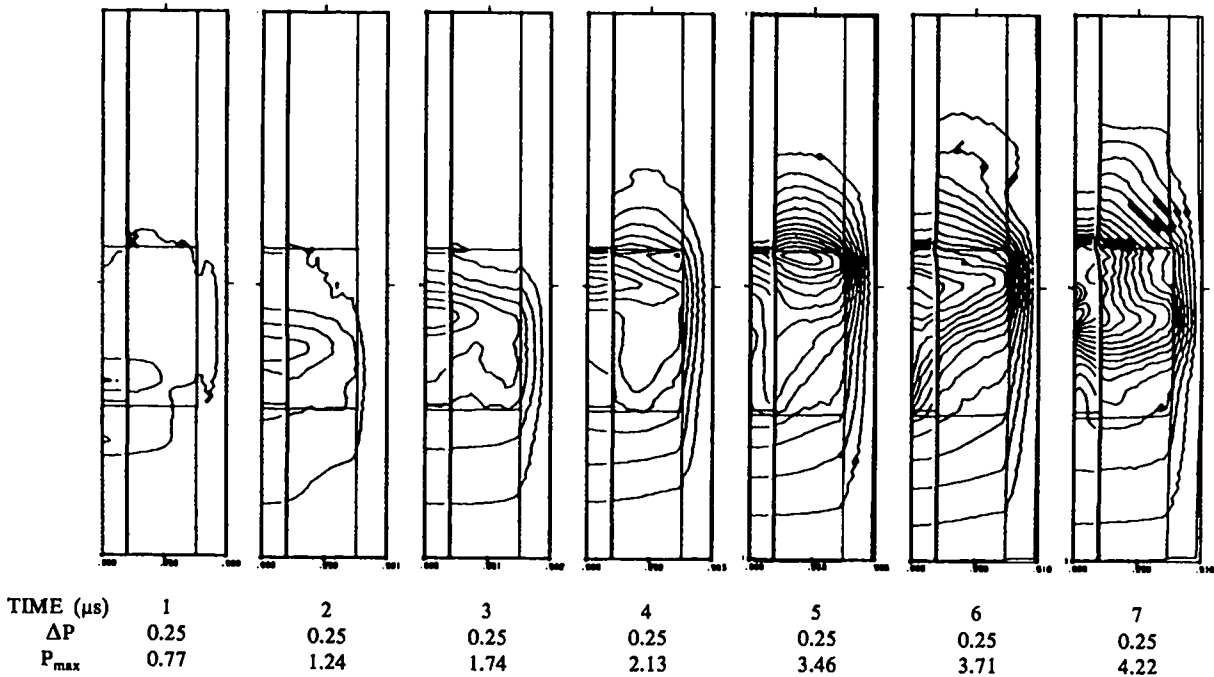


Fig. 9b.
 Pressure contours. Ignition velocity = 0.20 cm/ μs and $(S/V)_0 = 400/\text{cm}$. ΔP = contour interval (kbar). P_{max} = maximum pressure (kbar).

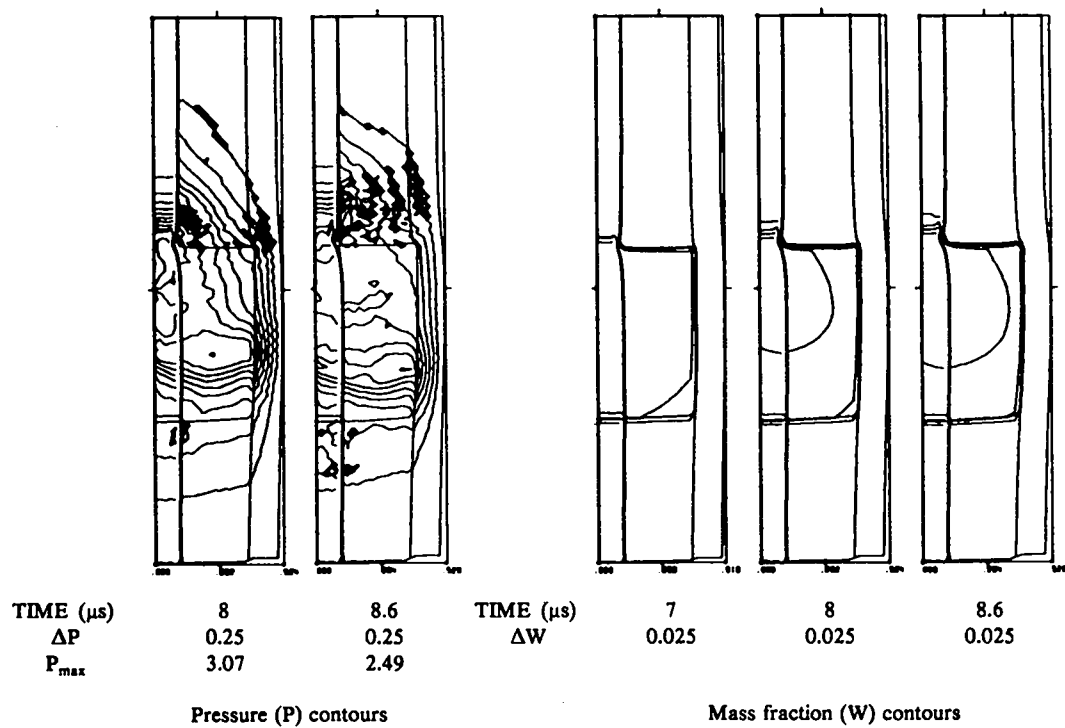


Fig. 9b. (cont)

Ignition velocity = 0.20 cm/ μ s and $(S/V)_0 = 400$ /cm. ΔP = contour interval (kbar). ΔW = contour interval fraction. P_{max} = maximum pressure (kbar).

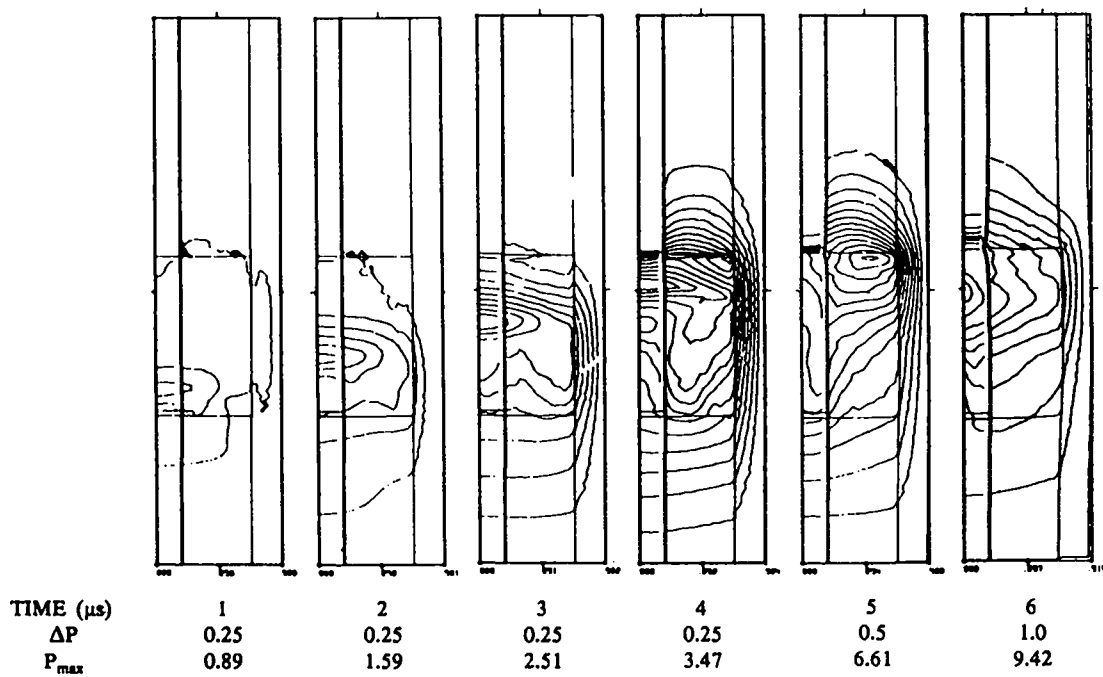


Fig. 9c.

Pressure contours. Ignition velocity = 0.20 cm/ μ s and $(S/V)_0 = 500$ /cm. ΔP = contour interval (kbar). P_{max} = maximum pressure (kbar).

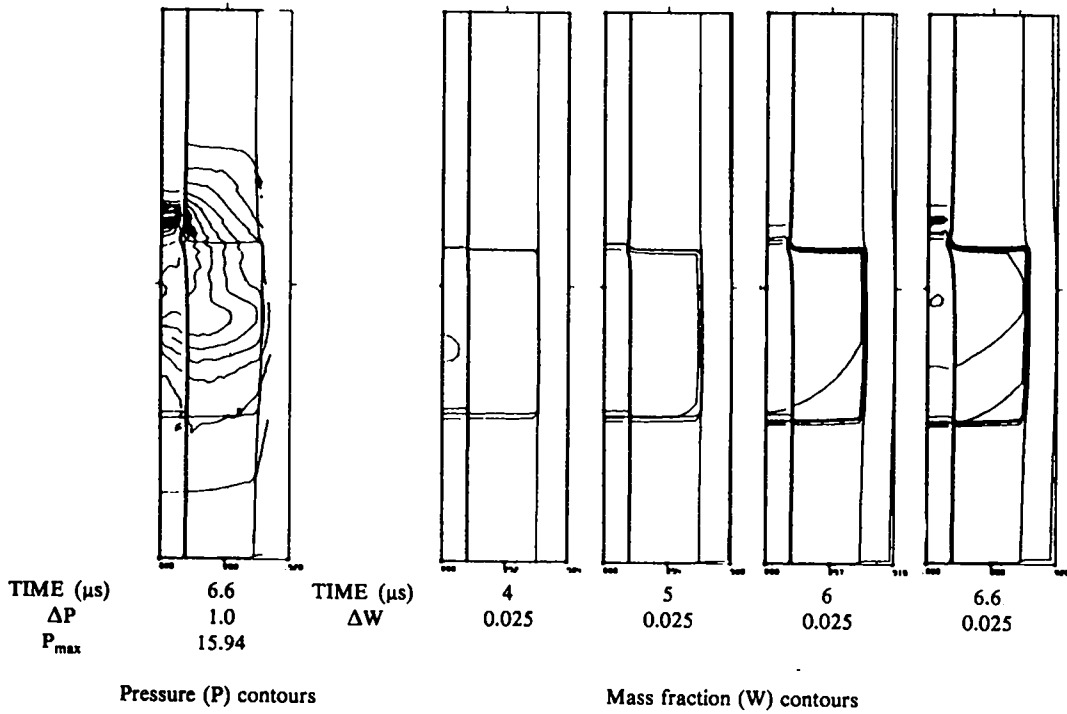


Fig. 9c. (cont)
 Ignition velocity = 0.20 cm/ μ s and $(S/V)_0 = 500/cm$. ΔP = contour interval (kbar). ΔW = contour interval fraction. P_{max} = maximum pressure (kbar).

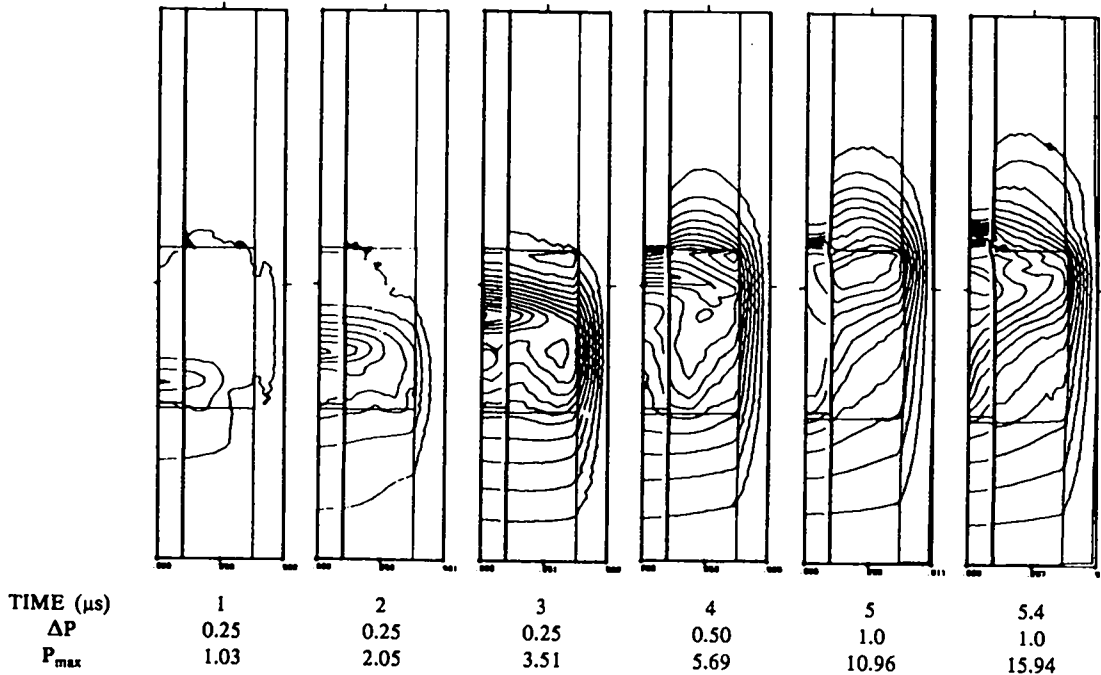


Fig. 9d.
 Pressure contours. Ignition velocity = 0.20 cm/ μ s and $(S/V)_0 = 600/cm$. ΔP = contour interval (kbar). P_{max} = maximum pressure (kbar).

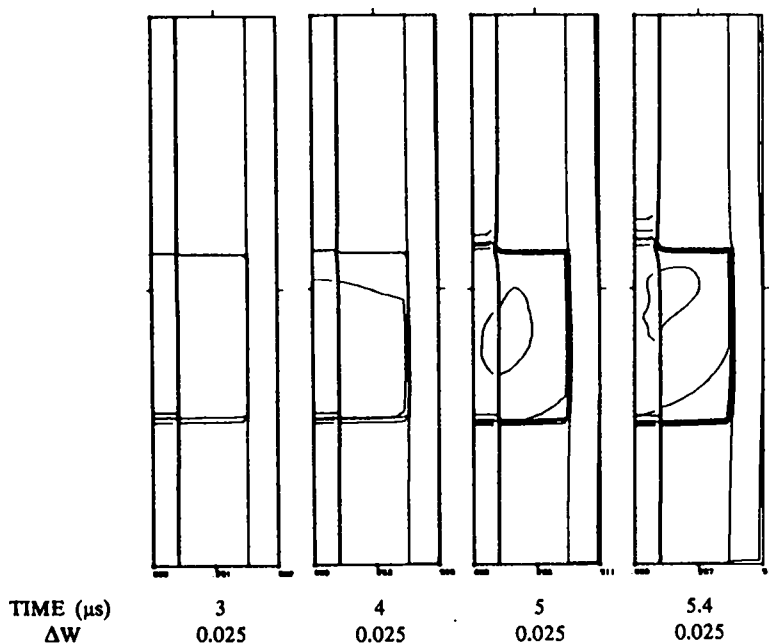


Fig. 9d. (cont)
 Mass fraction (W) contours. Ignition velocity = 0.20 cm/μs and
 $(S/V)_0 = 600/\text{cm}$. $\Delta W = \text{contour interval fraction}$.

TABLE VI
 CALCULATION SETS—FIGURE NUMBERS

Ignition Velocity (cm/μs)	Ignition Front Plot (Figure No.)	Pressure-Mass Fraction Plots ^a (Figure No.)				
		(S/V) Ratio (1/cm)				
		200	400	500	600	800
0.05	7a		7b	7c	7d	
0.10	8a	8b	8c	8d	8e	8f
0.20	9a		9b	9c	9d	

^aFigure numbers in boxes (□) show no prompt detonation and a decreasing maximum pressure at late times in the calculation.

The steel transition tube effect can be seen especially in Figs. 8c and 8d, where there is a high-pressure annulus directly below the steel, just as the ignition front reaches the end of the donor charge. The center transition charge is compressed and relieves the pressure below it in the donor charge. At later times, case expansion is significant and drops the pressure radially, giving a maximum pressure at the center of the donor charge.

The ignition velocity is expected to be less than the sound speed; in 1.70-g/cm³ PETN the sound speed is about 0.14 cm/μs. The ignition velocities of 0.05 and 0.10 cm/μs may be physically possible and the 0.20 cm/μs may not be, but it was included to display the model sensitivity to this variable. Because no ignition mechanism is in the model and because ignition may require much longer than allowed times, the ignition

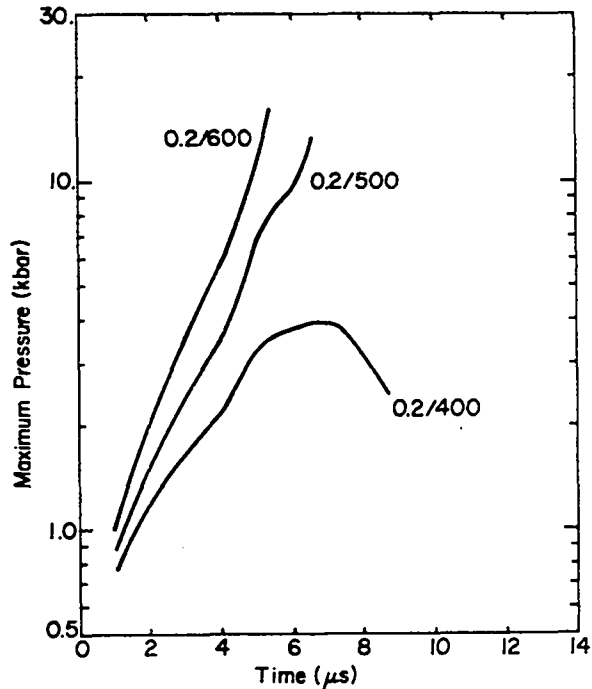
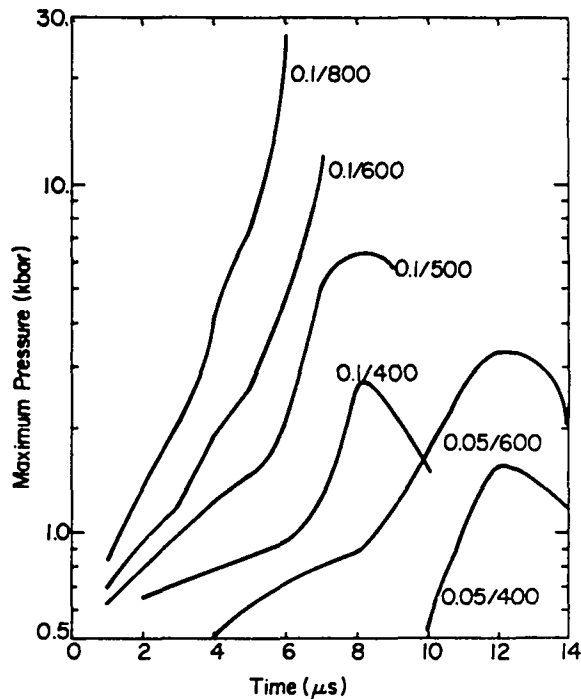


Fig. 10.

Calculated maximum pressure as a function of time. The pairs of numbers labeling the curves are ignition velocity (cm/μs) and initial surface-to-volume ratio (1/cm).

front may be considered better as the onset of rapid burning following ignition.

The required surface-to-volume ratios are small compared to the surface-to-volume ratios of the PETN powder used experimentally to make the explosive pressings. The powders used have (S/V)'s of 6200 and 15 000/cm. The value of (S/V) = 600/cm corresponds to that of 0.01-cm cubes and (S/V) = 60/cm corresponds to 0.1-cm cubes. Such particles are 10 to 20 times larger than the pressing powder particles. Pressing the powder to higher densities used in the donor charge eliminates much of the available surface of the original powder.

ACKNOWLEDGMENTS

I gratefully acknowledge the helpful discussions with Robert Dinegar and Charles Mader of the Los Alamos National Laboratory.

REFERENCES

1. Robert H. Dinegar and Daniel T. Varley III, "All-Secondary Explosive Hot-Wire Devices," Los Alamos Scientific Laboratory report LA-7897-MS (October 1979).
2. Charles L. Mader, *Numerical Modeling of Detonations* (University of California Press, 1979).
3. Charles A. Forest, "Burning and Detonation," Los Alamos Scientific Laboratory report LA-7245 (July 1978).
4. B. N. Kondrikov, V. M. Raikova, and B. S. Samsonov, "Kinetics of the Combustion of Nitro Compounds at High Pressures," *Combustion, Explosion, and Shock Waves* 9, 68-73 (1974) (a Plenum Pub. Corp. translation of *Fizika Goreniya I Vzryva*).

5. Charles L. Mader and Charles A. Forest, "Two-Dimensional Homogeneous and Heterogeneous Detonation Wave Propagation," Los Alamos Scientific Laboratory report LA-6259 (June 1976).
6. J. B. Ramsay and A. Popolato, "Analysis of Shock Wave and Initiation Data for Solid Explosives," in *Fourth Symposium (International) on Detonation*, White Oak, Maryland, Office of Naval Research Symposium report ACR-126 (1966).
7. Charles L. Mader and Milton Samuel Shaw, "User's Manual for SIN," Los Alamos Scientific Laboratory report LA-7264-M (September 1978).
8. John M. Walsh and Russell H. Christian, "Equation of State of Metals from Shock Wave Measurements," *Phys. Rev.* **97**, 1544 (1955).
9. Charles L. Mader, "FORTRAN BKW: A Code for Computing the Detonation Properties of Explosives," Los Alamos Scientific Laboratory report LA-3704 (July 1967).
10. Charles L. Mader, "Detonation Properties of Condensed Explosives Computed Using the Becker-Kistiakowsky-Wilson Equation of State," Los Alamos Scientific Laboratory report LA-2900 (July 1963).
11. Dante Stirpe, James O. Johnson, and Jerry Wackerle, "Shock Initiation of XTX-8003 and Pressed PETN," *J. Appl. Phys.* **41**, 3884 (1970).
12. G. E. Seay and L. B. Seely, Jr., "Initiation of a Low-Density PETN Pressing by a Plane Shock Wave," *J. Appl. Phys.* **32**, 1092 (1961).
13. Terry R. Gibbs and Alphonse Popolato, Eds., *LASL Explosive Property Data*, (University of California Press, 1980).
14. Bart Olinger and Howard Cady, "The Hydrostatic Compression of Explosives and Detonation Products to 10 GPa (100 kbars) and Their Calculated Shock Compression: Results for PETN, TATB, CO₂, and H₂O," in *Sixth Symposium (International) on Detonation*, Office of Naval Research Symposium report ACR-221 (1976), pp. 700-709.

Printed in the United States of America
 Available from
 National Technical Information Service
 US Department of Commerce
 5285 Port Royal Road
 Springfield, VA 22161
 Microfiche \$3.50 (A01)

Page Range	Domestic Price	NTIS Price Code	Page Range	Domestic Price	NTIS Price Code	Page Range	Domestic Price	NTIS Price Code	Page Range	Domestic Price	NTIS Price Code
001-025	\$ 5.00	A02	151-175	\$11.00	A08	301-325	\$17.00	A14	451-475	\$23.00	A20
026-050	6.00	A03	176-200	12.00	A09	326-350	18.00	A15	476-500	24.00	A21
051-075	7.00	A04	201-225	13.00	A10	351-375	19.00	A16	501-525	25.00	A22
076-100	8.00	A05	226-250	14.00	A11	376-400	20.00	A17	526-550	26.00	A23
101-125	9.00	A06	251-275	15.00	A12	401-425	21.00	A18	551-575	27.00	A24
126-150	10.00	A07	276-300	16.00	A13	426-450	22.00	A19	576-600	28.00	A25
									601-up	†	A99

†Add \$1.00 for each additional 25-page increment or portion thereof from 601 pages up.